

Raman Identification of Inclusions in Diamond

Evan M. Smith

*Gemological Institute of America
New York, NY 10036
USA*

evan.smith@gia.edu

Mandy Y. Krebs

*Department of Renewable Resources
University of Alberta
Edmonton, AB T6G 2H1
Canada*

krebs@ualberta.ca

Philomena-Theresa Genzel, Frank E. Brenker

*Department of Geosciences
Goethe University Frankfurt
60438 Frankfurt
Germany*

INTRODUCTION

Diamonds and their inclusions are some of the most scientifically valuable samples of the Earth (Haggerty 1999; Shirey et al. 2019). Among the analytical techniques used to study diamonds, Raman spectroscopy offers several advantages that make it an appealing tool for characterizing inclusions. It is a relatively low-cost, rapid, and non-destructive option, requiring minimal sample preparation, if any. Inclusions can often be characterized in-situ, while still fully enclosed in their diamond host, which ensures that no material is inadvertently lost (e.g., fluid) and the remnant pressure of the inclusion–host system is preserved. The pressure within inclusions can be on the order of several gigapascals (e.g., Nasdala et al. 2003) and is especially important for stabilizing the crystal structure of certain high-pressure minerals, such as ringwoodite, in sublithospheric diamonds (Pearson et al. 2014). Ideally, Raman spectroscopy can be complemented by other in-situ methods, such as infrared spectroscopy (FTIR), micro-beam X-ray diffraction (XRD), X-ray computed tomography (CT), and synchrotron X-ray fluorescence (XRF). Raman spectroscopy can serve as a first step to help characterize inclusions before employing more time-consuming or destructive analytical techniques, but it can also serve as a powerful tool in its own right for diamond research (e.g., Liu et al. 1990; Gillet et al. 2002; Nasdala et al. 2003, 2005; Brenker et al. 2005; Walter et al. 2011; Howell et al. 2012; Pearson et al. 2014; Nimis et al. 2016; Smit et al. 2016; Smith et al. 2016b, 2018; Anzolini et al. 2018; Kemppinen et al. 2018). This chapter is the first Raman spectroscopy review specifically applied to inclusions in diamond.

Collecting Raman spectra can be straightforward, often with little training for users. However, obtaining good quality data and making reasonable interpretations can be challenging

and varies with each application of Raman spectroscopy. This chapter provides an overview of the application of Raman spectroscopy to inclusions in diamond, with a focus on highlighting relevant phases likely to be encountered in this context. A collection of Raman spectra is available as supplementary material (Smith 2021), intended to provide a diamond-specific resource for identifying included phases. Many but not all of these spectra come from inclusions in diamond. For some minerals, spectra from inclusions are not available or available spectra collected from non-inclusion samples are higher quality and more representative, making them better suited for use as a reference. Additional spectral databases, from the RRUFF Project (Lafuente et al. 2015) for example, can be found online, although users should be mindful of occasional erroneous data. With the correct mineralogical parameters, Raman spectra can also be predicted from first principles, such as in the WURM database of computed spectra, which sometimes can be useful for identifying Raman peak distributions of an unknown mineral phase (Caracas and Bobocioiu 2011). Helpful background information on Raman spectroscopy and its geological applications can be found in reviews elsewhere (e.g., Burke 2001; Fries and Steele 2010; Frezzotti et al. 2012; Neuville et al. 2014; Elements 2020).

PRINCIPLES AND METHODS

Raman spectroscopy

When visible light intercepts matter, some of the light is scattered. Although most of the scatter occurs elastically, meaning the photon energy (or wavelength) remains unchanged, a small proportion of photons (approximately 1 in 10^7) scatter inelastically and their energy is measurably changed (Pasteris and Beyssac 2020). This is the Raman effect. The energy change, or Raman shift, is a consequence of some energy being transferred into (Stokes) or being released from (anti-Stokes) the vibrations of bonded atoms in the light-scattering material. This means that the spectrum of all the inelastically scattered photon energies is not random, but has bands (also called peaks) that correspond to the discrete vibrational frequencies in the material (i.e., the sample).

Raman spectroscopy exploits this phenomenon, whereby the spectrum of inelastically scattered light contains structural and, to some extent, chemical information about the sample. Typically, a laser source with photons of uniform energy is focused onto the sample and the scattered light is collected. The intense elastic scattering of the incident laser wavelength is excluded or removed from the signal using a Rayleigh rejection filter, triple monochromator or, in the case of a Fourier Transform system, an interferometer. It is important to note that the Raman shift is relative to the incident photon energy, meaning the energy or wavelength of a Raman band depends on the laser wavelength. For this reason, Raman spectra are plotted on a wavenumber-shift or Raman shift scale, which shows the energy change of scattered photons *relative* to the incident laser photons (in units of cm^{-1}). This is not to be confused with an *absolute* wavenumber scale of energy (conventionally used for infrared absorption spectroscopy).

Instrumentation and sample considerations

The basic Raman spectrometer (or Raman microprobe) consists of a laser light source, a microscope, and a spectrometer. In the context of examining inclusions in diamonds, an important variable to consider is the use of a confocal arrangement of the optical pathway (e.g., Everall 2009). A two-dimensional confocal aperture blocks out-of-focus light, constraining the effectively analyzed sample volume and improving spatial resolution. A quasi-confocal arrangement can be achieved using a slit rather than an aperture. The spatial resolution also depends on how tightly the objective lens focuses the laser, which is a function of the lens's numerical aperture (NA) and the laser excitation wavelength (λ), and is proportional to λ/NA . For example, with a confocal setup, a 0.9 NA, 100 \times magnification objective lens and 514.5 nm

laser can achieve a spatial resolution of approximately $1 \times 1 \times 5 \mu\text{m}^3$, elongate in the vertical axis (i.e., the axis of the incident laser beam). Note, however, that there are many additional factors affecting the spatial resolution (e.g., Kim et al. 2020) and that focusing the laser inside the diamond will further distort the spatial resolution due to refraction, surface roughness, and other effects. Ideally, inclusions should be as close to the surface of the diamond as possible, but realistically, they are often hundreds of micrometers deep or more and the working distance becomes an issue. For this reason, long working distance lenses are practical, at 100×, 50× or 20× magnification, for example, and can permit analysis of inclusions as deep as a few millimeters. Long working distance lenses have the tradeoff of a lower NA (e.g., a 50× long working distance lens might have a NA of 0.5), which increases the analyzed volume, chiefly in the vertical dimension because the height of the analyzed volume is inversely proportional to the square of the NA. This lowers the spatial resolution and can result in a diminished Raman signal intensity from the inclusion of interest.

The choice of laser is also important. Blue, green, and red lasers can all be used with varying success depending on the sample. Shorter wavelengths lead to smaller spot sizes and more intense Raman scattering, but the drawback is an increased likelihood of fluorescence from the diamond (or inclusion) that may drown out the Raman signal and decrease spectral resolution. Heating of the inclusion by the laser spot is not normally a concern, but it is possible and measures such as reducing the laser power may be prudent for sensitive hydrous or opaque phases. Smaller grain sizes and coexistence with phases that act as insulators are also factors that can facilitate heating. In this sense, Raman spectroscopy is not always non-destructive (e.g., de Faria et al. 1997). When striving to avoid damage, a good approach is to start at the lowest laser power and iteratively work up to a point where the Raman signal strength is acceptable. If possible, measuring the laser at the sample using a power meter is preferable. Additional factors such as the depth of the inclusion will affect the laser power reaching the inclusion.

It is possible to analyze through rough diamond surfaces, especially smooth and flat crystal or cleavage surfaces. Generally, the better an inclusion can be resolved visually, the greater the chances of being able to analyze it. A well-polished diamond surface (facet or window) is therefore ideal and becomes increasingly important for inclusions that are smaller or located deeper inside the diamond. If polishing is to be pursued, it may be helpful to collect X-ray CT images to locate all inclusions to aid planning, although this has the potential for a high radiation dose that could affect the sample. During polishing, good technique is important to avoid excessive sample heating, which could hypothetically modify or destabilize sensitive inclusions, such as hydrous ringwoodite.

When using a Raman microscope, good control over the lighting conditions is critical for navigating the subsurface space inside a diamond to find specific inclusions or parts of inclusions and bring them into focus for analysis. Transmitted light, with a diffuser plate or frosted microscope slide, or even an external light source, such as an intense fiber optic light, can be especially helpful. Depending on the sample, it can be possible to analyze inclusions even smaller than $1 \mu\text{m}$, although successfully targeting the laser on the inclusion can present a challenge and the Raman signal may be weak. If a sufficiently dense cloud of inclusions is present, it can be possible to train the spot on the cloud and have a good chance of intersecting inclusions (e.g., Navon et al. 2017). Alternatively, when small inclusions are more dispersed, an automated mapping approach with a small step size can sequentially analyze a grid of many points and maximize the chances of hitting inclusions (e.g., Smit et al. 2016). Mapping capabilities are also helpful when analyzing multi-phase inclusions, where a traditional point analysis approach could allow some phases to go unnoticed, such as the presence of small amounts of molybdenite in sulfide inclusions (Kemppinen et al. 2018). Newer instruments capable of faster automated Raman mapping, in combination with the higher spatial resolution afforded by confocal optics, are likely to bolster the use of 2-D and 3-D mapping for inclusion analysis.

Common challenges

Diamond has a very strong first-order Raman band, located at 1332.5 cm^{-1} in relatively strain- and impurity-free crystals (Schiferl et al. 1997) (larger grains than the excitation beam diameter), which is conveniently isolated from the $100\text{--}1300\text{ cm}^{-1}$ region where the key spectral features of most minerals lie. However, the diamond host can still present a challenge to inclusion analysis when it luminesces, imparting a strong broad background that can drown out the Raman spectrum, or when it introduces more discrete photoluminescence bands into the spectrum. Laser-induced photoluminescence can sometimes be overcome by controlling the laser spot size to excite less of the diamond (Kemppinen et al. 2018), or attempting analysis again with a different laser wavelength, if possible. Photoluminescence from defects in the diamond lattice, which may sometimes occur only locally around an inclusion (e.g., Fig. 9 in Gu and Wang 2018), can produce bands at discrete wavelengths that overlap the Raman spectral features. It can be helpful to analyze the host diamond itself, adjacent to an inclusion of interest, for comparison. Also, photoluminescence features can be diagnosed by changing the laser excitation wavelength. These features depend on electronic transitions and will be detected at the same *absolute* energy or wavenumber, and therefore a different apparent Raman shift (wavenumber-shift), upon changing the laser wavelength. True Raman bands will plot at constant wavenumber-shift values, meaning their position in the Raman shift spectrum will not change upon changing the laser wavelength. Having the ability to choose between multiple laser wavelengths thus presents an advantage.

It is not uncommon for inclusions to contain multiple phases, which can be overlapped in Raman spectra, making phase identification more difficult. For example, this could occur as the result of co-trapping of multiple mineral grains together or as a result of retrogression of a single high-pressure mineral into multiple lower-pressure phases. Retrogression is a common phenomenon observed in sublithospheric diamonds. If an inclusion is not homogeneous, the Raman spectrum can exhibit substantial spatial variability and recognizing all the phases present can be difficult. Some phases may be very weakly active or even Raman inactive. Analyzing multiple points on the inclusion, potentially by automated mapping (e.g., Walter et al. 2011), is crucial to being able to recognize and deconvolve the spectra of mixed phases.

Another challenging aspect of inclusions in diamond is the presence of remnant pressure. As a diamond makes its way to Earth's surface, the changes in pressure and temperature allow the diamond to relax, but its inclusions are constrained by the host diamond. As a result, many inclusions are under residual stress, which can often be seen visually with crossed polarizing filters as a halo of anomalous birefringence in the diamond surrounding an inclusion (Howell et al. 2010). The remnant pressure can be on the order of a few gigapascals (Nasdala et al. 2003) and, rarely, might be greater than 10 GPa for some exotic micrometer- to nanometer-sized inclusions (Navon et al. 2017; Tschauer et al. 2018). The pressure can make it difficult to identify phases because residual pressure affects the bonding geometry and shifts the position of some Raman bands. For example, the main band of coesite in an unstrained state resides at 520.6 cm^{-1} but under high remnant pressure as an inclusion this band has been recorded at 538 cm^{-1} (Smith et al. 2018). The host diamond Raman band also shifts under stress (Grimsditch et al. 1978; Sharma et al. 1985), which can be exploited to map out the stress distribution around inclusions (Nasdala et al. 2003; Howell et al. 2012). As a final note of caution, mentioned by Nasdala and Schmidt (2020), Raman spectroscopy can be deceptively simple and does not always receive sufficient oversight by trained users, so it is important to keep in mind that not all published Raman results are reliable.

INCLUSION IDENTIFICATION

For most users, the principal goal is to identify the phase or phases that make up a visible inclusion in a diamond. Mineral inclusions are categorized below in terms of depth of origin (lithospheric and sublithospheric) and major host rock types. Lithospheric and sublithospheric diamonds are presented separately because the latter often change from their original high-pressure mineralogy to lower-pressure phases during exhumation from the mantle, adding a degree of complexity to their interpretation.

Phase identification is accomplished by carefully comparing band positions, intensities, and shapes against those of known spectra, a process that can be aided by software that can automatically select possible matches from a database. It is important to keep in mind that band positions may be shifted due to remnant pressure in inclusions and that relative band intensities of a crystal can change as a function of its orientation with respect to the incident laser and its polarization. For identifying inclusions in diamond, it is helpful to consider the most plausible candidates as those minerals and mineral assemblages that have been encountered previously (Tables 1 and 2). Our list is not exhaustive and does not include the various phases that have been observed in micro- or nano-scale inclusions (e.g., Logvinova et al. 2008; Kaminsky 2012) that are less conducive to Raman analysis. A collection of relevant Raman spectra, including examples collected in-situ from inclusions, is available as supplementary material (Smith 2021). As visual inspection of inclusions under a microscope is often integral to Raman analysis, users may wish to refer to published images to see some good examples of different inclusion types (e.g., Koivula 2000; Tappert and Tappert 2011). In addition to minerals, fluids or amorphous solids are also possible inclusions in diamond, and these too can often be identified from their Raman spectra. However, scrutiny is required and phase identification is not always possible based on Raman spectra alone.

Inclusions in lithospheric diamonds

Inclusions in diamonds from the continental lithospheric mantle are divided into three paragenetic associations, reflecting their host rocks: peridotitic (comprising lherzolitic, harzburgitic and wehrlitic parageneses), eclogitic, and websteritic (Stachel and Harris 2008). Diamond from websteritic sources is relatively uncommon, accounting for only about 2% of inclusion-bearing lithospheric diamonds, whereas peridotitic and eclogitic parageneses account for 65% and 33%, respectively (Stachel 2014). Mineral phases encountered in lithospheric diamonds are laid out in Table 1 (also see Table 1 in Shirey et al. 2013) and some examples of corresponding Raman spectra from inclusions are shown in Figure 1. These inclusions are often single mineral phases and correspond to familiar minerals encountered in crustal rocks. As long as a reasonable Raman spectrum is collected, the identification of these phases is usually straightforward. In contrast, inclusions in sublithospheric diamonds often contain coexisting minerals representing a retrogression assemblage and may contain obscure mineral phases, adding a greater challenge to identification and interpretation.

Inclusions in sublithospheric diamonds

Inclusions derived from the sublithospheric mantle broadly mirror the peridotitic and eclogitic host rock associations of lithospheric diamond suites, but with mineralogy dictated by higher pressures and temperatures (see reviews by Stachel et al. 2005; Harte 2010; Kaminsky 2012; Harte and Hudson 2013; Shirey et al. 2013; Nestola 2017). The mineralogy of peridotitic and eclogitic rocks as a function of depth, which has been delineated experimentally, provide a practical guide for interpreting inclusions in sublithospheric diamonds (e.g., Walter et al. 2011). Although the high-pressure mineralogy of peridotitic or eclogitic bulk compositions does explain many inclusion assemblages in sublithospheric diamonds, there are also inclusions that deviate from this framework, such as the occurrence of carbonates, or of Ca-silicate inclusions

Table 1. Mineral inclusions in lithospheric diamond, modified from Stachel (2014).

Peridotitic	Eclogitic	Websteritic	Uncertain
<i>Common</i>			
Cr-pyrope	Grossular–almandine–pyrope	Almandine-pyrope	Graphite
Olivine	Omphacitic clinopyroxene	Diopside-augite	
Enstatite	Fe sulfides*	Enstatite	
Cr-diopside			
Mg-chromite			
Fe–Ni sulfides*			
<i>Occasional</i>			
	Rutile	Coesite	
	Coesite	Olivine	
<i>Rare</i>			
Coesite	Kyanite	Phlogopite	Diamond
Mg-ilmenite	Corundum		Calcite
Magnesite	Ilmenite		Dolomite
Calcite	Magnetite		Perovskite
Native Fe	Fe–Mg-chromite		Amphibole
Zircon	Phlogopite		Moissanite
Phlogopite	K-feldspar		Apatite
Yimengite	Titanite		Eskolaite
	Staurolite		Sr-titanate
	Zircon		Monazite
	Moissanite		
	Calcite		
	Dolomite		

Notes: *pyrrhotite ± pentlandite ± chalcopyrite ± molybdenite (Kemppinen et al. 2018), with bulk Ni content being >17 wt% for peridotitic and <10 wt% for eclogitic sulfides

with Ca:Si ratios above 1:1 that cannot be interpreted simply as a back-transformation product of CaSiO₃-perovskite (Brenker et al. 2005, 2007). Other host rock types, such as subducted serpentinites or oceanic sediments, may also be relevant for sublithospheric diamond formation. In detail, many sublithospheric inclusions do not appear to be pristine grains of ambient mantle rocks, but instead bear evidence of variable chemical modification by, or crystallization from, low-degree melts or fluids prior to their entrapment in diamond, possibly related to diamond formation (Stachel et al. 2000; Walter et al. 2008; Thomson et al. 2016).

Table 2 lists mineral phases encountered in sublithospheric diamonds and some examples of their Raman spectra are shown Figure 2. It should be noted that few inclusions are found as well-preserved high-pressure minerals. The large pressure-temperature change during exhumation from the sublithospheric mantle destabilizes some mineral inclusions, causing inversion (change in structure) or retrogression (breakdown into multiple phases) to lower-pressure polymorphs or assemblages. Observed inclusion phases must be carefully interpreted to judge the identity of the original inclusion phase that was trapped during diamond growth (also see Table 2 in Shirey et al. 2013). For example, inclusions of bridgmanite (MgSiO₃-perovskite) invert to orthopyroxene, but the original inclusion identity can be inferred based on

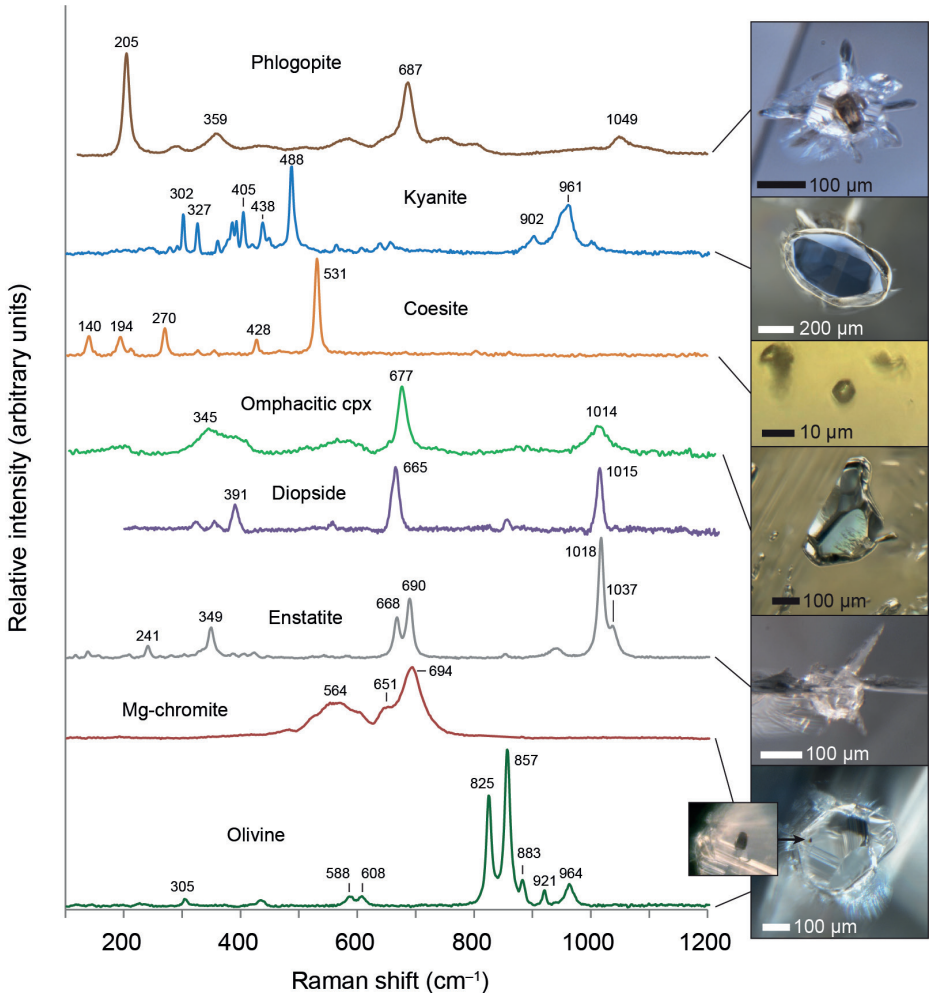


Figure 1. Raman spectra of a variety of mineral inclusions in lithospheric diamonds, along with corresponding inclusion images. The phlogopite inclusion, which also has an O–H stretching band at 3732 cm^{-1} , is in a faceted diamond (sample 110206866925) that also contains olivine inclusions. The kyanite inclusion is in a faceted diamond (sample 110209083424) that also contains orange eclogitic garnet inclusions. The coesite inclusion is in a yellow faceted diamond (sample 110208419590) and exhibits pressure-induced band shifts (Smith et al. 2016a). The omphacitic clinopyroxene (cpx) inclusion is in a yellow-green faceted diamond (sample 890000082714) that also contains orange eclogitic garnet (Fig. 3) inclusions (Smith and Wang 2017). The diopside inclusion (no image) is in a diamond from Sao Luiz (Juina area), Brazil. The enstatite is in a faceted diamond (sample 110208779832). The Mg-chromite is a small ($\sim 10\text{ }\mu\text{m}$) inclusion trapped within a larger forsteritic olivine inclusion in a faceted diamond (sample 100722703657).

low NiO contents (300 ppm or less) compared to typical upper mantle orthopyroxene (1000 ppm or more) (Stachel et al. 2005). Sometimes bridgmanite contains Al, and the inclusion undergoes retrogression to an assemblage of orthopyroxene plus aluminous phases, such as jeffbenite and spinel (Walter et al. 2011; Harte and Hudson 2013). Jeffbenite $[(\text{Mg,Fe})_3\text{Al}_2\text{Si}_3\text{O}_{12}]$, formerly known as TAPP (tetragonal almandine-pyrope phase), may appear by retrogression of aluminous bridgmanite or majoritic garnet, though its possible occurrence as an original/

Table 2. Mineral inclusions observed in sublithospheric diamonds, adapted from Harte and Hudson (2013) and Stachel (2014).

Single or multi-phase mineral inclusion	Possible original inclusion phase
<i>Common</i>	
*Ferropericlaise–magnesiowüstite	
Ca-rich inclusions: Breyite (CaSiO ₃ -walstromite), larnite (β-Ca ₂ SiO ₄), CaSi ₂ O ₅ -titanite, wollastonite, pseudowollastonite, perovskite (CaTiO ₃), titanite (CaTiSiO ₅), ZrO ₂ , (additional Ca-silicates?)	Various: CaSiO ₃ -perovskite (or Ca(Si,Ti)O ₃), breyite, larnite, CaSi ₂ O ₅ -titanite
Majoritic garnet ± cpx, olivine, plagioclase	Majoritic garnet
Jeffbenite	Majoritic garnet? Bridgmanite?
Jeffbenite + NaAl-pyroxene	Majoritic garnet
Olivine	Olivine, wadsleyite, ringwoodite
Quartz or coesite ± kyanite	Stishovite
Nepheline, spinel ± olivine	CF phase
Kalsilite, nepheline, spinel ± cpx	NAL phase
Opx ± jeffbenite, spinel, ilmenite, olivine, cpx	Bridgmanite (may be Al-bearing)
*Omphacitic cpx	
<i>Rarer occurrences</i>	
CaSiO ₃ -perovskite ± perovskite (CaTiO ₃)	Ca(Si,Ti)O ₃ -perovskite
K-feldspar	Liebermannite
Ca-feldspar	Stöfflerite
Calcite	Aragonite
*Ringwoodite	
*Phase Egg	
*Sulfides	
*Merwinite	
*Magnesite	
*Ilmenite	
*Corundum	
*Chromite	
*Spinel	
*Native Fe–Ni	
*Siderite	
*Titanite	

Note: *Inferred as the original inclusion phase, without inversion/retrogression. Abbreviations: opx = orthopyroxene; cpx = clinopyroxene; CF = Calcium-ferrite-structured phase; NAL = New aluminous phase.

primary inclusion is not ruled out (Nestola et al. 2016). Retrogression reactions can be complex, especially if multiple high-pressure phases have been trapped together (e.g., Brenker et al. 2002). Consequently, it is not always possible to accurately interpret the original inclusion mineralogy without additional tools beyond Raman spectroscopy.

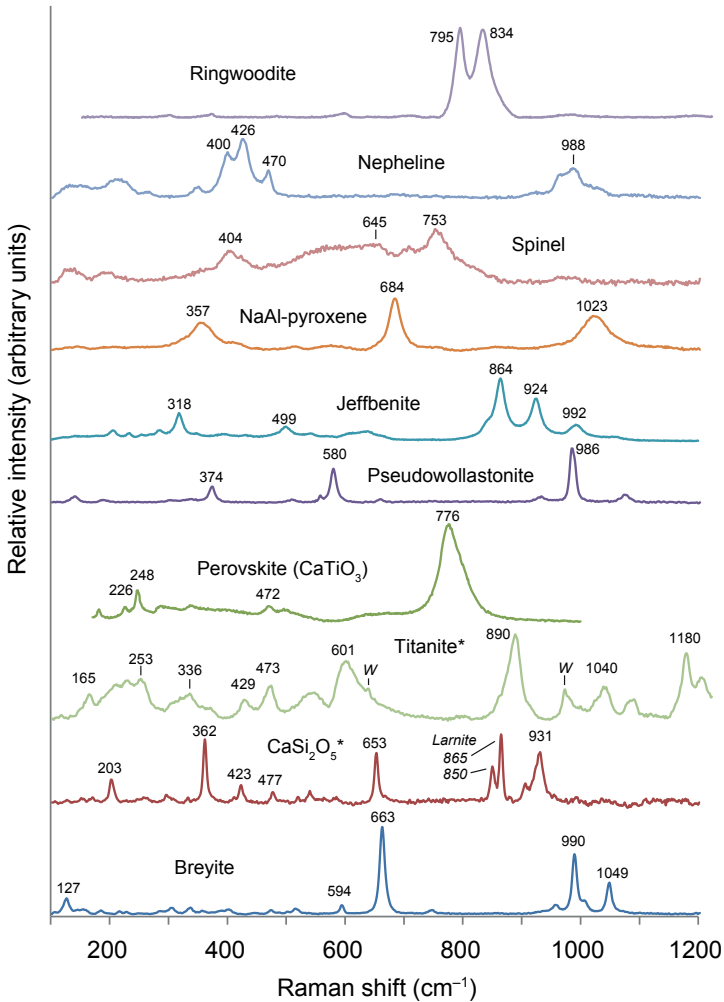


Figure 2. Raman spectra of a variety of phases included in sublithospheric diamonds. The ringwoodite shown is a synthetic crystal, R090003 from RRUFF (Lafuente et al. 2015). Nepheline and spinel were found coexisting in a multiphase inclusion in a boron-bearing (Type IIb) diamond (sample 110208245246 in Smith et al. 2018). NaAl-pyroxene was found as part of a composite inclusion with jeffbenite in a Type IIb diamond (sample 880000037816 in Smith et al. 2018). The jeffbenite shown is in a diamond from Sao Luiz (Juina area), Brazil (Nestola et al. 2016). Phases related to Ca- and Ca,Ti-silicate inclusions are pseudowollastonite (composite with breyite in sample 110208423120), perovskite (composite with CaSiO_3 -perovskite) (Nestola et al. 2018), titanite (composition uncertain) with wollastonite (bands labeled W) in the same analyzed volume (coexisting with other Ca-silicates in sample 100918637486), CaSi_2O_5 (structure uncertain) with larnite in the same analyzed volume (sample 110208104790), and breyite (sample 880000037816). (*There may be two different CaSi_2O_5 polymorphs, one with monoclinic (titanite-structured) and one with triclinic structure.) Note that olivine, kyanite, coesite, diopside, and enstatite (orthopyroxene) from Figure 1 are also important phases for sublithospheric diamonds.

Interpretation of the depth of origin and the likely host rock association can be made on the basis of assemblages of coexisting inclusions (Stachel et al. 2005; Harte 2010; Kaminsky 2012; Harte and Hudson 2013; Shirey et al. 2013; Nestola 2017). Caution is required, as some inclusions that are common in sublithospheric diamonds provide ambiguous depth

information when found as lone occurrences. Ferropericlyase, for example, is found among inclusion assemblages representing host rocks with peridotitic composition in the lower mantle (deeper than 660 km), but ferropericlyase inclusions on their own do not indicate a lower mantle origin (Stachel et al. 2005). Regions of low silica activity in the upper mantle can stabilize ferropericlyase (Brey et al. 2004). Similar care is required for lone inclusions of breyite, which cannot be automatically assumed to originate from CaSiO_3 -perovskite in the transition zone to lower mantle (Woodland et al. 2020; Brenker et al. 2021).

Remarks on some specific inclusion types

Graphite. Graphite is a common occurrence in diamond, sometimes as protogenetic, euhedral crystals (Nasdala et al. 2005) and possibly as a metastable syngenetic phase (Smit et al. 2016), but more often as a result of decompression in fractures surrounding inclusions, such as around sulfide inclusions. In addition to the most intense G band ($\sim 1580\text{ cm}^{-1}$), as well as the D and 2D bands of graphite, a weak but sharp band at 867 cm^{-1} that corresponds to “forbidden” out-of-plane vibrations (Kawashima and Katagiri 1999) is occasionally observed in graphitic material in inclusions.

In Raman spectroscopy, the presence of graphite can be helpful when analyzing inclusions that happen to be weak or Raman inactive, because detecting graphite from around the inclusion confirms that spectral information is, in fact, being collected from the inclusion. In this case, finding no discernible Raman spectrum from the major volume of the inclusion itself can be a useful observation.

Distinguishing among garnets. Garnet is widespread in the lithosphere, asthenosphere, and mantle transition zone and it is regularly found as an inclusion in diamond. In general, most garnet inclusions have similar features (Fig. 3) but their spectra change as a function of composition (Kolesov and Geiger 1998) and structural disorder. It is possible to determine garnet compositions by considering their spectral features as linear combinations between end-members (Bersani et al. 2009). For diamond, Kalugina and Zedgenizov (2020) have evaluated suites of eclogitic and peridotitic garnet inclusions and found reasonable agreement between compositions measured by EPMA analysis and compositions estimated from Raman spectra using the approach of Bersani et al. (2009). Kalugina and Zedgenizov (2020) used the rotation ($\text{R}[\text{SiO}_4]$) and stretching (Si-O) vibrations of SiO_4 -tetrahedra near 360 and 910 cm^{-1} , respectively, to estimate relative molar proportions of pyrope, almandine, and grossular. For their samples, $\text{R}[\text{SiO}_4]$ was the most sensitive band position, with eclogitic garnet inclusions falling within $355.9\text{--}361.2\text{ cm}^{-1}$ and peridotitic garnet inclusions being within $361.2\text{--}365.2\text{ cm}^{-1}$ (Kalugina and Zedgenizov 2020). This difference in $\text{R}[\text{SiO}_4]$ band position mainly reflects the difference in contribution from almandine and pyrope end-members at 342 cm^{-1} and 364 cm^{-1} , respectively (Kolesov and Geiger 1998).

It can also be possible to recognize majoritic garnet (i.e., garnet from the sublithospheric mantle, with more than 3 Si per formula unit), from the width of the strongest Raman mode near 910 cm^{-1} (McMillan et al. 1989). Gillet et al. (2002) proposed that widened bands (FWHM greater than about 25 cm^{-1}) are due to disorder of Al, Mg, and Si at the octahedral sites in majoritic garnet and can be considered diagnostic. If a garnet were to exhibit grain sizes smaller than the excitation laser beam diameter, this could also cause broadening. Narrower bands, however, do not necessarily rule out a majoritic component.

Sulfides. Sulfide inclusions can often be recognized visually, by their metallic grey or yellowish appearance and black graphitic fracture rosettes. The major sulfide phase, pyrrhotite, is only weakly Raman active and is usually not observable by Raman in-situ. Bands at about 376 cm^{-1} and 341 cm^{-1} are associated with monoclinic pyrrhotite (Fig. 4), but can vary with Fe/S ratio and structure (Hope et al. 2001), whereas hexagonal pyrrhotite may be inactive (Mernagh and Trudu 1993). Pentlandite (main band at 370 cm^{-1}) and chalcopyrite in sulfide

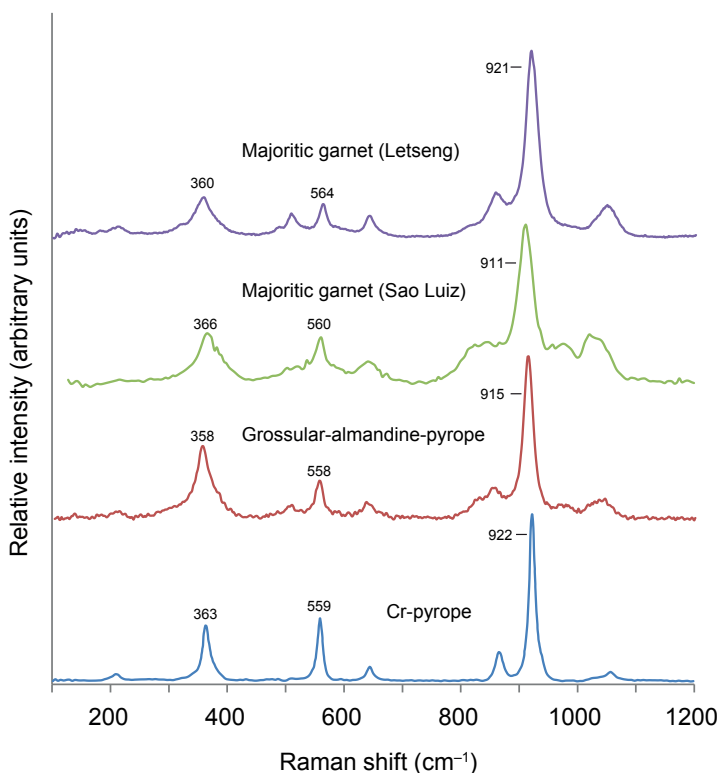


Figure 3. Examples of Raman spectra from garnet inclusions in diamond. Majoritic garnets in diamonds from Letseng (sample 110207974892 in Smith et al. 2016b) and Sao Luiz (sample BZ43 in Gillet et al. 2002) have broadening of the strongest band and some additional weak and broad underlying features between 800 and 1000 cm^{-1} . The lithospheric garnet inclusions grossular–almandine–pyrope (sample 110209083424) and Cr-pyrope (Siberian diamond sample in Kalugina and Zedgenizov 2020) may potentially be distinguished from one another based on the position of the $\sim 360 \text{ cm}^{-1}$ band (Kalugina and Zedgenizov 2020).

inclusions can also be difficult to detect. Studies on sulfide inclusions have more often relied on exposing the inclusion to characterize it. However, a recent Raman-based identification of small amounts of molybdenite in a significant number of sulfide inclusions in diamonds from several localities has led to the suggestion that Raman should be used as part of the initial characterization of sulfides prior to Re–Os dating studies (Kemppinen et al. 2018). Molybdenite and chalcopyrite (Fig. 4) are more Raman active and are detected more easily than pyrrhotite and pentlandite.

Calcium silicates. Calcium silicate inclusions, most notably breyite (Brenker et al. 2021; CaSiO_3 -walstromite), have popularly been interpreted as a breakdown product from more or less pure CaSiO_3 -perovskite, which is part of the experimentally-predicted mineralogy of the lower part of the transition zone and lower mantle for almost all rock types, including peridotitic, eclogitic and most sedimentary bulk compositions (e.g., Irifune and Ringwood 1987, 1993). A single example of non-inverted CaSiO_3 -perovskite in diamond shows that the entrapment of CaSiO_3 -perovskite indeed occurs, although, unfortunately, CaTiO_3 - and CaSiO_3 -perovskite seem to show almost indistinguishable Raman spectra (Nestola et al. 2018). In detail, however, most calcium silicate inclusions are more complicated (Brenker et al. 2021) and exhibit multiple phases (Brenker et al. 2005). Their interpretation as a breakdown product from CaSiO_3 -perovskite should not be automatic.

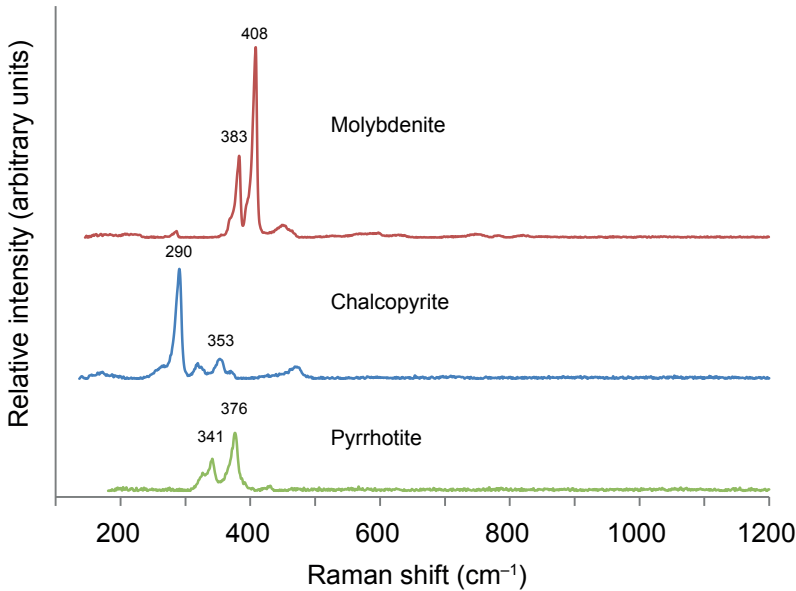


Figure 4. Raman spectra of phases found in sulfide inclusions in diamond. Sulfides can be challenging to characterize by Raman spectroscopy, but it has been suggested as a useful way to check for the presence of molybdenite, which may be important for Re–Os geochronology studies (Kempainen et al. 2018). Pyrrhotite (R060440), chalcopyrite (R050018), and molybdenite (R060124) are from RRUFF (Lafuente et al. 2015).

For a long time, it was presumed that a pure CaSiO_3 phase would not be stable in any likely mantle rock composition at depths shallower than about 520 km. However, on the basis of inclusions in diamond, Brenker et al. (2005) have demonstrated that Ca,Si-rich environments exist in the sublithospheric mantle and that these regions can enable the formation and entrapment of breyite in diamond at depths of less than 300 km.

In some instances, a simple CaSiO_3 precursor is precluded by bulk inclusion Ca:Si ratios that are markedly different from 1:1 (Brenker et al. 2005). If diamond is formed in the lower part of the transition zone or lower mantle, CaSiO_3 -perovskite might be captured together with stishovite (SiO_2) if a basaltic or sedimentary precursor is assumed. In this case the Ca:Si ratio of the whole inclusion will be lower than 1:1. However, it was experimentally demonstrated that breyite could crystallize together with diamond in the upper mantle (at 6–10 GPa) in SiO_2 -rich compositions (Woodland et al. 2020) resulting in the same phase assemblage.

For inclusions with a bulk Ca:Si ratio above 1:1, which usually consist of coexisting breyite and larnite ($\beta\text{-Ca}_2\text{SiO}_4$), the interpretation is less straightforward. In this case, diamond crystallization in the lower mantle is unlikely for peridotitic or basaltic bulk compositions. In order to account for such an inclusion, the diamond could have formed at conditions corresponding to the two-phase stability field of larnite and CaSi_2O_5 -titanite. Here, a high Ca:Si ratio could be achieved by capturing a higher amount of larnite relative to CaSi_2O_5 -titanite, breyite or CaSiO_3 -perovskite. The formation depth in this case will be between 300 and 400 km, that is, in the upper mantle above the transition zone. Furthermore, Fedoraeva et al. (2019) have experimentally shown that with an aragonite-breyite starting assemblage, an assemblage of breyite-larnite can be formed at 6 GPa and about 1700 °C due to incongruent melting, which again is at upper mantle conditions. Considering these possibilities, it is clear that the finding of breyite (with or without other Ca-silicates) inclusions alone as an inclusion in diamond does not necessarily indicate a transition zone or lower mantle depth (Brenker et al. 2021).

Besides breyite, a surprising number of different calcium silicates can sometimes be found in inclusions, even co-existing metastably (Table 2). Some uncertainty surrounds the Raman identification of CaSi_2O_5 -titanite. Two different CaSi_2O_5 polymorphs have been observed in high pressure experimental products, corresponding to monoclinic (titanite-structure) and triclinic structures (Angel 1997; Kubo et al. 1997; Kudoh and Kanzaki 1998; Akaogi et al. 2004). In some experiments, monoclinic CaSi_2O_5 -titanite produced at high pressure has inverted to the triclinic structure upon decompression (Akaogi et al. 2004). It might therefore be expected that both CaSi_2O_5 polymorphs could potentially be found in calcium silicate inclusions in diamond (compare $\text{CaSi}_2\text{O}_5^*$ and titanite* in Fig. 2).

The Raman spectrum corresponding to a synthetic CaSi_2O_5 sample produced by Gasparik et al. (1994) has been reported as CaSi_2O_5 -titanite ($\text{CaSi}_2\text{O}_5^*$ in Fig. 2) in multi-phase calcium silicate inclusions (Nasdala et al. 2003; Anzolini et al. 2016; Smith et al. 2016b). However, it is not clear if the crystal structure of this sample, after decompression, has been verified as monoclinic CaSi_2O_5 -titanite or if it might potentially be the triclinic polymorph.

In some multi-phase calcium silicate inclusions, a Raman spectrum resembling true monoclinic titanite (CaTiSiO_5) with a prominent band at $\sim 600\text{ cm}^{-1}$ (titanite* in Fig. 2) has been recorded (Smith et al. 2017). The composition of this phase was not determined, but based on the observation that the Raman spectra of CaSiO_3 -perovskite and CaTiO_3 -perovskite might be virtually indistinguishable (Nestola et al. 2018), it is considered possible that the spectra of CaSi_2O_5 -titanite and true titanite (CaTiSiO_5) are similar. If so, the CaSi_2O_5 sample of Gasparik et al. is not actually in the titanite structure but in the triclinic structure.

With the variety of calcium silicates described in diamonds to date, it may be reasonable to expect some additional phases to be encountered in future studies. Wollastonite-II, for instance, has been found in multiphase carbonatitic microinclusions (Kaminsky et al. 2009), and could potentially be part of larger calcium silicate inclusions. However, it may not be readily distinguishable from breyite by Raman spectroscopy, because their crystal structures are nearly identical (Joswig et al. 2003; Dörsam et al. 2009; Barkley et al. 2011). Some other phases that may be important for Ca-rich inclusion investigations are rankinite ($\text{Ca}_3\text{Si}_2\text{O}_7$), kilchoanite ($\text{Ca}_3\text{Si}_2\text{O}_7$), hartrurite/post-hartrurite (Ca_3SiO_5), tilleyite/post-tilleyite ($\text{Ca}_5\text{Si}_2\text{O}_7(\text{CO}_3)_2$), trabzonite ($\text{Ca}_4(\text{Si}_3\text{O}_5\text{OH})\text{OH}$), and chegemite ($\text{Ca}_7(\text{SiO}_4)_3(\text{OH})_2$), as well as hydrous post-hartrurite, hydrous larnite, and hydrous CaSiO_3 -perovskite (e.g., Németh et al. 2017).

Ferropericlaise–magnesiowüstite. Inclusions of ferropericlaise–magnesiowüstite are one of the most commonly reported phases in sublithospheric diamonds. This phase is often transparent and brown, but can possess a colorful iridescence at the inclusion surface that is a good indicator for identification (Fig. 5). Inclusions can exhibit a wide range of $\text{Mg}/(\text{Mg}+\text{Fe})$ ratios, but most are within 0.60–0.82 (Stachel et al. 2005). For simplicity, the term ferropericlaise is sometimes applied to the whole ferropericlaise–magnesiowüstite series in inclusions.

Pure periclaise (MgO) is Raman inactive, whereas wüstite (FeO) is weakly active with one somewhat broad band near 652 cm^{-1} (de Faria et al. 1997). The Raman spectra of periclaise–wüstite solid solutions have not been studied. As there is no accepted Raman spectrum for ferropericlaise, a Raman-based identification is strictly not possible. However, ferropericlaise inclusions whose identities have been confirmed using other techniques do exhibit some consistent Raman features. Figure 5 shows Raman spectra associated with confirmed (Fig. 5a–f) and inferred (Fig. 5g) ferropericlaise inclusions in diamond, though the exact assignment of these features is uncertain. The ferropericlaise inclusions in one of these diamonds (Fig. 5d–f) have also been identified by both EPMA analysis ($\text{Mg}/(\text{Mg}+\text{Fe}) = 0.91$) and X-ray diffraction (Smith et al. 2018). The possibility of exsolved magnesioferrite within ferropericlaise inclusions (e.g., Palot et al. 2016) may be important, although the spectra in Figure 5 do not resemble magnesioferrite (e.g., D’Ippolito et al. 2015). One possibility is that the features are related

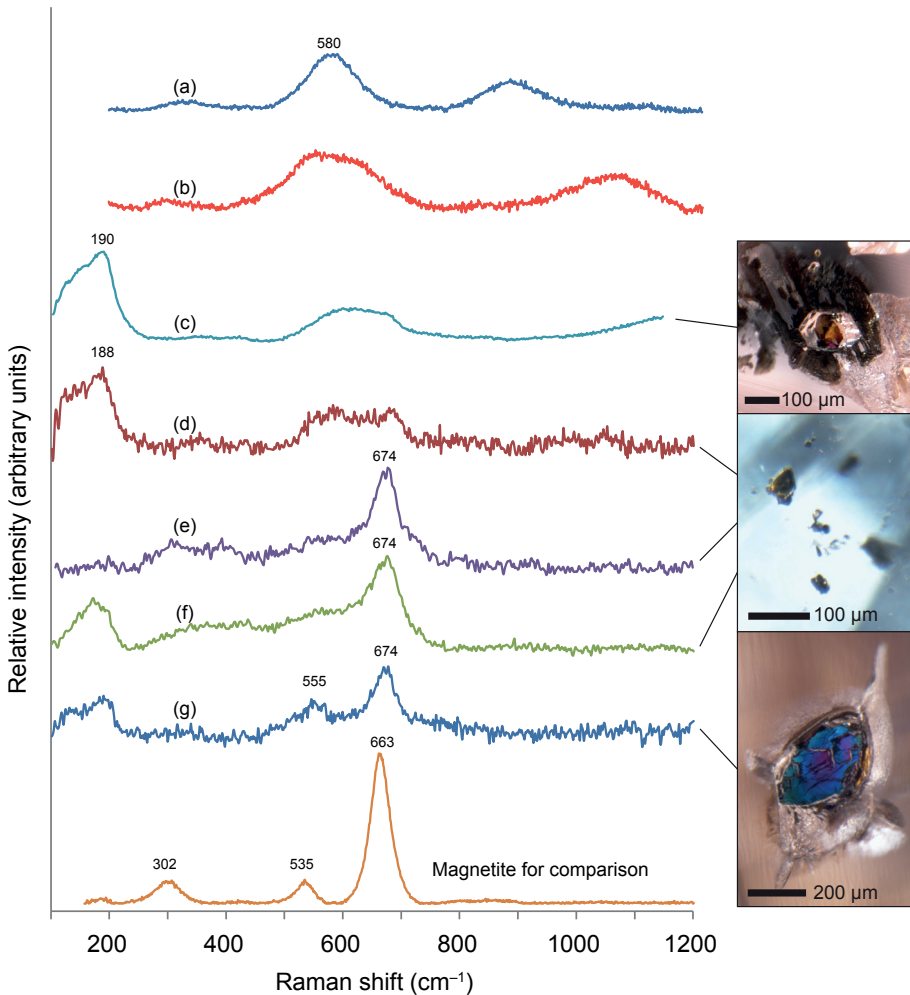


Figure 5. Raman spectra tentatively associated with ferropierclase inclusions. The spectral features themselves may not necessarily belong to ferropierclase. **(a)** Ferropierclase inclusion in a diamond from Juina, Brazil. **(b)** Ferropierclase in a diamond from Sao Luiz (Juina area), Brazil. **(c)** Ferropierclase in a pink-brown diamond (sample CBP-0937) also containing two-phase composite inclusions of breyite and CaTiO_3 -perovskite. This spectrum was collected from an exposed surface after breaking open the inclusion. **(d, e, f)** Three spectra collected from different inclusions in a boron-bearing (Type IIb) diamond (sample 110208425476 in Smith et al. 2018). **(g)** Large and iridescent inferred ferropierclase in a faceted pink diamond (sample 110206861072). Magnetite reference spectrum R080025 from RRUFF (Lafuente et al. 2015).

to magnetite (shown in Fig. 5). Laser-induced decomposition during Raman analysis could potentially cause ferropierclase to break down at the inclusion surface to produce magnetite, similar to the destabilization of wüstite noted by de Faria et al. (1997) that was found to produce α -Fe and magnetite (Fe_3O_4) under intense laser excitation. It may also be possible to partially destabilize ferropierclase by overheating the diamond during polishing. Alternatively, ferropierclase inclusions can potentially contain naturally-occurring micro-exsolutions of metal and magnetite (Anzolini et al. 2020). Further study is needed to characterize the Raman spectrum of ferropierclase inclusions.

Metallic melt inclusions. A recently recognized variety of sublithospheric diamonds, called CLIPPIR diamonds, contain metallic Fe–Ni–C–S melt as their most abundant inclusion (Smith et al. 2016b, 2017). These inclusions were trapped as liquid, so are technically not mineral inclusions and are not listed in Table 2. However, they deserve mention in the discussion of sublithospheric diamonds. Although not well-represented in the geological literature from inclusion studies, many inclusion-free, nitrogen-deficient (Type IIa) diamonds can tentatively be assigned to the CLIPPIR category, in which case they may account for approximately 1% of the gem marketplace (Smith et al. 2017). The physical characteristics of CLIPPIR diamonds, often being colorless, large, and inclusion-poor, place them among the most valuable gem diamonds, seldom accessible for research.

The Fe–Ni–C–S metallic melt inclusions solidify to an assemblage of cohenite, pyrrhotite, and Fe–Ni alloy (\pm minor Fe–Cr-oxide, Fe-phosphate) (Smith et al. 2016b, 2017). These phases are virtually undetectable by Raman spectroscopy in-situ. However, Raman spectroscopy can still be helpful to increase the confidence in identifying them, beyond visual recognition. It is often possible to detect methane (as sharp band around 2915–2918 cm^{-1}), and sometimes molecular hydrogen, at the inclusion-diamond interface (Smith et al. 2016b, 2017). However, methane has also been recorded in other kinds of inclusions in diamond (Smit et al. 2016) and is not diagnostic of Fe–Ni–C–S metallic inclusions. Similar metallic melt inclusions, potentially of variable composition, have been observed more rarely in sublithospheric Type IIb (boron-bearing) diamonds (Smith et al. 2018). Various inclusions with native Fe, Ni, Fe–Ni alloys, and Fe-carbides have also been described in other kinds of sublithospheric diamonds, although it is unclear if these are related to the recurring Fe–Ni–C–S melt found in CLIPPIR diamonds (Hayman et al. 2005; Bulanova et al. 2010; Gurney et al. 2010; Kaminsky and Wirth 2011).

Additional high-pressure phases

As mentioned above, high-pressure phases are commonly found as retrograde transformation products and only a handful of mineral inclusions with their original mineralogy intact have been reported. One such mineral is ringwoodite, the most dominant mineral at the lower part of the mantle transition zone (~520–660 km depth) (e.g., Irifune and Ringwood 1987), which was first synthesized in Fe_2SiO_4 composition in 1958 (Ringwood 1958) and not long after discovered in the Tenham L6-chondrite (Binns et al. 1969). The first terrestrial sample, however, has only recently been found, as an inclusion in diamond, and was first identified using Raman spectroscopy (Pearson et al. 2014). Thus, while finding pristine high-pressure phases as inclusions in diamond is rare, it is possible, and Raman spectroscopy is an ideal tool to identify them. Unfortunately, not all experimentally derived phases have published Raman spectra. An example is the Al-rich phases expected to form in basaltic/eclogitic bulk compositions at lower mantle conditions, called NAL (new aluminous) phase (e.g., Akaogi et al. 1999; Gasparik et al. 2000) and CF (calcium-ferrite type structure) phase (e.g., Irifune and Ringwood 1993; Hirose et al. 2005; Ono et al. 2005), that are listed as possible original inclusions in Table 2. However, our spectral database (Smith 2021) includes a number of other possible deep mantle phases, from experiments and meteorites studies, that could plausibly occur in diamonds and the most important ones are introduced in this section.

Wadsleyite. While ringwoodite has been found in diamond, wadsleyite, the high-pressure equivalent of olivine replacing it as the principal rock-forming mineral below the 410 km discontinuity (e.g., Irifune and Ringwood 1987) in the upper portion of the mantle transition zone, has not yet been found. Because the entrapment conditions of high-pressure inclusions observed in terrestrial diamonds extend well within the stability of field of wadsleyite (Navon et al. 2017; Tschauner et al. 2018), researchers are actively searching for a pristine specimen.

Dense hydrous magnesium silicates. Experimental studies have shown that a number of dense hydrous magnesium silicates (DHMS) are stable at mantle pressures, corresponding

to depths greater than ~200 km (e.g., Ohtani et al. 2005; Komabayashi and Omori 2006). These phases are denoted by alphabetical names (e.g., A, B, etc.) and are expected to form either within deeply subducted cold slabs by metamorphism of serpentinites or within the convecting mantle by metasomatism from slab-derived hydrous fluid (Tschauner 2019). The DHMS phases proposed to be relevant to sublithospheric diamond formation (Harte 2010) are phase A, phase E, superhydrous phase B, and phase D (Litasov and Ohtani 2007 and references therein). Serpentinites and DHMS phases formed from them have further been suggested as potential carriers of water and boron for the formation of Type IIb diamonds in the transition zone and lower mantle (Smith et al. 2018).

Sediment assemblages. Geochemical, geophysical and experimental studies have shown evidence suggesting the subduction of continental crust and terrigenous and pelagic sediments to the mantle transition zone and possibly even to the lower mantle, despite their relative buoyancy compared to the surrounding mantle (e.g., von Huene and Scholl 1991; Irifune et al. 1994; Workman et al. 2004; Afonso and Zlotnik 2011). Once this material reaches depths greater than 250–300 km, its density increases significantly due to the formation of dense silicates, marking a “point of no return” for subducted continental crust. The volume of continental material that can be subducted is mainly dependent on the rheology of the continental crust, with strong crusts favoring deep subduction.

Based on experimental work on the phase relations in dry and hydrous sediment systems at transition zone and lower mantle pressures and temperatures, summarized by Litasov and Ohtani (2007), as yet undiscovered high-pressure minerals stable at such depths are liebermannite (KAlSi_3O_8 -hollandite) and zagamiite (CAS phase). Liebermannite (Urakawa et al. 1994; Ma et al. 2018) is considered to be the most abundant phase in a continental crust bulk composition at pressure and temperature conditions corresponding to the mantle transition zone (Irifune et al. 1994). While both liebermannite and zagamiite (Gautron et al. 1996; Beck et al. 2004; Ma et al. 2018) have been found in shocked meteorites but not as terrestrial samples, one inclusion in diamond (Kankan, Guinea) has been reported where liebermannite might have been the precursor (Stachel et al. 2000). In hydrous sediment systems, two additional experimentally predicted phases are topaz-OH and δ -AlOOH (Wunder et al. 1993, 1999; Suzuki et al. 2000; Ohtani et al. 2001; Xue et al. 2006, 2010). Topaz-OH is thought to be stable above the mantle transition zone, between 250–350 km, while δ -AlOOH is expected to be a breakdown product of *phase egg*, along with stishovite, at depths below 450 km.

Tuite. Tuite (γ - $\text{Ca}_3(\text{PO}_4)_2$) is the main product formed from apatite, a common accessory mineral occurring in a variety of terrestrial rocks, at high pressures and has been shown to be stable at upper and lower mantle conditions (Murayama et al. 1986; Zhai et al. 2013). The natural occurrence of tuite was first found in the Suizhou L6 chondrite (Xie et al. 2003). The apatite-tuite transformation has been shown experimentally in both apatite–MORB (Konzett and Frost 2009) and apatite–peridotite (Konzett et al. 2011) systems, but so far no terrestrial samples have been discovered.

VOLATILE COMPONENTS

In addition to detecting characteristic vibrations from mineral phases, Raman spectroscopy is well-suited for detecting liquids or gases trapped as inclusions in diamond. Mineral inclusions in diamond can sometimes have small amounts of fluid coexisting with the main solid portion of the inclusion. For example, based on Raman analyses, it has been found that some common inclusions in lithospheric diamonds are surrounded by a thin layer ($< 1.5 \mu\text{m}$) of hydrous silicic fluid that contains $\text{Si}_2\text{O}(\text{OH})_6$, $\text{Si}(\text{OH})_4$, and molecular H_2O (Nimis et al. 2016). Inclusions in some sublithospheric diamonds also possess an invisible fluid layer, made up of CH_4 , with or without H_2 (Smith et al. 2016b, 2018) and possibly other species.

The ferropericlasite inclusion shown in Figure 5g even has a layer of CH₄. Methane has also been found associated with graphite in mixed-habit diamonds from Marange (Smit et al. 2016).

Fluid and melt inclusions have been reported along healed cracks in diamond, in which case Raman spectroscopy has revealed N₂ and CO₂ in the fluids (Tomilenko et al. 2001; Smith et al. 2014, 2015). Nitrogen has also been recorded in solid form, as nano-inclusions in some sublithospheric diamonds, where it is proposed to have exsolved from the substitutional nitrogen in the diamond lattice (Rudloff-Grund et al. 2016; Navon et al. 2017). Reviews on Raman analysis of fluid inclusions are a useful resource for characterizing volatile species (e.g., Burke 2001; Frezzotti et al. 2012; Bodnar and Frezzotti 2020).

RAMAN BAROMETRY

At the moment of entrapment, an inclusion is assumed to be enclosed by the host without any anomalous stresses at the interface (i.e., a uniform uninterrupted stress state with no squeezing or stretching and a perfect geometrical fit between the inclusion and host). When a diamond is carried to Earth's surface, it can relax freely in response to the change in pressure and temperature, but its inclusions are nearly fixed in volume and are unable to expand freely. As a result, many inclusions are under considerable remnant pressures, reaching a few gigapascals (e.g., Nasdala et al. 2003).

Raman spectra can provide barometric information of the host-inclusion system because crystal lattice strains distort bonds, thereby changing vibrational frequencies and the position of Raman bands. It is possible to quantify the remnant pressure in an inclusion if a calibration is available for pressure-induced band shifts for the included phase, having the same chemical composition and structure (e.g., Sobolev et al. 2000; Gillet et al. 2002; Nasdala et al. 2003). By combining this remnant pressure with thermoelastic parameters of the mineral inclusion and the diamond host, it is possible to constrain the pressure–temperature conditions of diamond formation (Israeli et al. 1999; Angel et al. 2014, 2015; Anzolini et al. 2018). Software such as EoSFit-Pinc (Angel et al. 2017) is useful for this purpose. However, non-elastic behavior of the diamond host around the inclusion, due to brittle or plastic deformation, can effectively alleviate some inclusion pressure, leading to underestimation of the depth of diamond growth (Howell et al. 2012).

Some additional obstacles limit this technique. The simplest inclusion would be a sphere, with isotropic properties, trapped in a host with isotropic properties. A somewhat equant, round shaped inclusion of a cubic mineral trapped in diamond (also cubic) is a reasonable approximation of the ideal scenario (Howell et al. 2010). Care must be taken when examining pressures in anisotropic mineral inclusions in diamond because of the possibility for deviatoric stresses that will lead to Raman band shifts that do not follow congruently with hydrostatic pressure calibrations (Anzolini et al. 2018). There is currently no reliable method among existing analytical techniques and hydrostatic calibrations to determine strains in minerals subject to deviatoric stresses and interpret them in terms of a single “inclusion pressure.” Another issue is that strains and Raman shifts can vary spatially within an inclusion, which is exacerbated by anisotropy and the effects of inclusion geometry (Mazzucchelli et al. 2018). In these cases, the center of the inclusion, away from edges, provides the best measurement for calculating entrapment conditions (Murri et al. 2018).

Host diamond barometry

Distortion of the host diamond around inclusions can be easily observed using crossed polarizers. This anomalous birefringence can be used to gage residual pressure and the distribution of strains in a diamond (Howell et al. 2010). The distortions also affect both the position and width of its main Raman band, normally located at 1332.5 cm⁻¹ (also often stated as 1332 cm⁻¹) in relatively strain- and impurity-free diamond (Schiferl et al. 1997).

Growth patterns and bulk deformation features of the whole diamond can also be manifested in spatial variations of the diamond Raman features. The distribution of strain around an inclusion is highly variable, but Raman mapping has been successfully applied to reveal its maxima/minima and geometry (Nasdala et al. 2003; Howell et al. 2012). Pressure exerted on the diamond in the $\langle 111 \rangle$ axis (perpendicular to one of its octahedral planes) causes a band shift of $+0.7 \text{ cm}^{-1}/\text{GPa}$ and along the $\langle 001 \rangle$ axis (perpendicular to one of its cube planes) a band shift of $+2.2 \text{ cm}^{-1}/\text{GPa}$ (Grimsditch et al. 1978; Sharma et al. 1985). As the crystallographic direction is relevant for the band shift calibration, it is necessary to understand the geometry of stresses and Raman analysis in order to quantify pressure adjacent to an inclusion (Nasdala et al. 2003). The band shift of the diamond adjacent to an inclusion can nevertheless provide some indication of remnant pressure inside the inclusion.

Inclusion barometry

Using Raman spectroscopy, the pressure has been quantified in several kinds of inclusions in diamond, such as coesite, olivine, clinopyroxene, garnet, breyite, and solid nitrogen (Liu et al. 1990; Izraeli et al. 1999; Sobolev et al. 2000; Gillet et al. 2002; Nasdala et al. 2003; Barron et al. 2008; Howell et al. 2012; Smith et al. 2015; Navon et al. 2017; Anzolini et al. 2018).

Coesite. The strongest band of coesite at 520.6 cm^{-1} in an unstressed crystal shifts by $+2.9 (\pm 0.1) \text{ cm}^{-1}/\text{GPa}$ under hydrostatic compression (Hemley 1987). Beginning with Sobolev et al. (2000), this calibrated pressure-induced band shift has been used for inclusion barometry in several studies. It is good practice to check multiple coesite bands to ensure they exhibit similar pressure-induced shifts in their position (e.g., Table 3 in Hemley 1987). Otherwise, if the band shifts are incoherent, it suggests anisotropic stresses and the shift of the 520.6 cm^{-1} band alone cannot be simply translated into an inclusion pressure. Calculation of trapping conditions of coesite inclusions based on remnant pressure often yields depths shallower than the diamond stability field, possibly due to anisotropic effects or plastic deformation around inclusions (Howell et al. 2010).

Breyite. An experimental calibration of pressure-induced Raman shifts up to 7.5 GPa under hydrostatic conditions was accompanied by ab initio calculations to assess the influence of non-hydrostatic conditions (Anzolini et al. 2018). The latter considerations revealed that some bands in the spectrum are more strongly influenced by non-hydrostatic conditions than others. The 977 cm^{-1} band of breyite was proposed to be the least sensitive to deviatoric stresses and most appropriate for determining the residual pressure, using its calibrated shift of $+5.16(\pm 0.09) \text{ cm}^{-1} / \text{GPa}$ (Anzolini et al. 2018). It is notable that although many breyite inclusions are interpreted to be of sublithospheric origin in the transition zone or lower mantle, the remnant pressures in most breyite inclusions are relatively modest. The greatest band shifts yet observed in breyite inclusions are only sufficient to constrain the minimum inclusion entrapment depth to about 240–280 km (Anzolini et al. 2018; Smith et al. 2018). Brittle and plastic deformation of the surrounding diamond host could be responsible for some of this discrepancy. Some inclusions also have textural evidence of expansion of inclusion material out into decompression cracks (e.g., Smith et al. 2017, 2018), which could violate the assumption of a constant inclusion volume.

CONCLUDING REMARKS

Raman spectroscopy is well-suited as a reconnaissance tool for inclusion characterization and can be complementary to other in-situ methods such as FTIR, micro-beam XRD, X-ray CT, and synchrotron-XRF. Basic identification of mineral inclusions is often straightforward, especially by referring to the spectra of those minerals that have been found previously in diamond, or even those that are anticipated to occur in the deep mantle based on high-

pressure experiments (Smith 2021). When used in conjunction with techniques to measure inclusion composition, such as EPMA analysis, or *in situ* with synchrotron-XRF (Laforce et al. 2014; De Pauw et al. 2020), Raman spectroscopy provides a simple way to confirm the crystal structure of mineral phases. The technique can also reveal hidden phases that might otherwise go unnoticed, such as molybdenite in sulfide inclusions (Kemppinen et al. 2018), or invisible layers of fluid trapped at the interface between solid inclusions and the host diamond (e.g., Nimis et al. 2016; Smith et al. 2018). In addition to identifying trapped phases, Raman data can reveal information about stresses in inclusions and permit calculation of minimum trapping conditions. The speed, low cost, minimal sample preparation, and capability to analyze inclusions *in-situ* make Raman spectroscopy a valuable method in the analytical toolkit for diamond research.

ACKNOWLEDGEMENTS

The authors wish to thank L. Nasdala and A. Steele for their careful reviews, as well as S. Shirey and K. Smit for their editorial handling. Thanks to F. Nestola for discussion and providing the spectrum for jeffbenite, and to P. Diggle for discussion. F.E.B. would like to thank the DFG (project BR2015/36-1) and the Dr. Rolf M. Schwiete Stiftung Foundation for financial support.

REFERENCES

- Afonso JC, Zlotnik S (2011) The subductability of continental lithosphere: the before and after story. *In*: Arc-Continent Collision, *Frontiers in Earth Sciences*. Vol 4. Brown D, Ryan PD (eds). Springer, Berlin, Heidelberg, p 53–86
- Akaogi M, Hamada Y, Suzuki T, Kobayashi M, Okada M (1999) High pressure transitions in the system $MgAl_2O_4$ – $CaAl_2O_4$: a new hexagonal aluminous phase with implication for the lower mantle. *Phys Earth Planet Inter* 115:67–77
- Akaogi M, Yano M, Tejima Y, Iijima M, Kojitani H (2004) High-pressure transitions of diopside and wollastonite: phase equilibria and thermochemistry of $CaMgSi_2O_6$, $CaSiO_3$ and $CaSi_2O_5$ – $CaTiSiO_5$ system. *Phys Earth Planet Inter* 143–144:145–156
- Angel R (1997) Transformation of fivefold-coordinated silicon to octahedral silicon in calcium silicate, $CaSi_2O_5$. *Am Mineral* 82:836–839
- Angel RJ, Mazzucchelli ML, Alvaro M, Nimis P, Nestola F (2014) Geobarometry from host-inclusion systems: The role of elastic relaxation. *Am Mineral* 99:2146–2149
- Angel R, Alvaro M, Nestola F, Mazzucchelli M (2015) Diamond thermoelastic properties and implications for determining the pressure of formation of diamond-inclusion systems. *Russ Geol Geophys* 56:211–220
- Angel RJ, Mazzucchelli ML, Alvaro M, Nestola F (2017) EosFit-Pinc: A simple GUI for host-inclusion elastic thermobarometry. *Am Mineral* 102:1957–1960
- Anzolini C, Angel R, Merlini M, Derzsi M, Tokár K, Milani S, Krebs M, Brenker F, Nestola F, Harris J (2016) Depth of formation of $CaSiO_3$ -walsstromite included in super-deep diamonds. *Lithos* 265:138–147
- Anzolini C, Prencipe M, Alvaro M, Romano C, Vona A, Lorenzon S, Smith EM, Brenker FE, Nestola F (2018) Depth of formation of super-deep diamonds: Raman barometry of $CaSiO_3$ -walsstromite inclusions. *Am Mineral* 103:69–74
- Anzolini C, Marquardt K, Stagno V, Bindi L, Frost DJ, Pearson DG, Harris JW, Hemley RJ, Nestola F (2020) Evidence for complex iron oxides in the deep mantle from FeNi(Cu) inclusions in superdeep diamond. *PNAS*:202004269
- Barkley MC, Downs RT, Yang H (2011) Structure of walsstromite, $BaCa_2Si_3O_9$, and its relationship to $CaSiO_3$ -walsstromite and wollastonite-II. *Am Mineral* 96:797
- Barron LM, Barron BJ, Mernagh TP, Birch WD (2008) Ultrahigh pressure macro diamonds from Copeton (New South Wales, Australia), based on Raman spectroscopy of inclusions. *Ore Geol Rev* 34:76–86
- Beck P, Gillet P, Gautron L, Daniel I, El Goresy A (2004) A new natural high-pressure (Na,Ca)-hexaluminosilicate $[(Ca_xNa_{1-x})Al_{3+x}Si_{3-x}O_{11}]$ in shocked Martian meteorites. *Earth Planet Sci Lett* 219:1–12
- Bersani D, Andò S, Vignola P, Moltifiori G, Marino I-G, Lottici PP, Diella V (2009) Micro-Raman spectroscopy as a routine tool for garnet analysis. *Spectrochim Acta Part A* 73:484–491
- Binns RA, Davis RJ, Reed SJB (1969) Ringwoodite, natural $(Mg,Fe)_2SiO_4$ spinel in the Tenham meteorite. *Nature* 221:943
- Bodnar RJ, Frezzotti ML (2020) Microscale chemistry: raman analysis of fluid and melt inclusions. *Elements* 16:93–98
- Brenker FE, Stachel T, Harris JW (2002) Exhumation of lower mantle inclusions in diamond: ATEM investigation of retrograde phase transitions, reactions and exsolution. *Earth Planet Sci Lett* 198:1–9

- Brenker FE, Vincze L, Vekemans B, Nasdala L, Stachel T, Vollmer C, Kersten M, Somogyi A, Adams F, Joswig W (2005) Detection of a Ca-rich lithology in the Earth's deep (> 300 km) convecting mantle. *Earth Planet Sci Lett* 236:579–587
- Brenker FE, Vollmer C, Vincze L, Vekemans B, Szymanski A, Janssens K, Szaloki I, Nasdala L, Joswig W, Kaminsky F (2007) Carbonates from the lower part of transition zone or even the lower mantle. *Earth Planet Sci Lett* 260:1–9
- Brenker FE, Nestola F, Brenker L, Peruzzo L, Harris JW (2021) Origin, properties and structure of breyite: The second most abundant mineral inclusion in super-deep diamonds. *Am Mineral* 106:38–43
- Brey GP, Bulatov V, Girmis A, Harris JW, Stachel T (2004) Ferropericlasite—a lower mantle phase in the upper mantle. *Lithos* 77:655–663
- Bulanova GP, Walter MJ, Smith CB, Kohn SC, Armstrong LS, Blundy J, Gobbo L (2010) Mineral inclusions in sublithospheric diamonds from Collier 4 kimberlite pipe, Juina, Brazil: Subducted protoliths, carbonated melts and primary kimberlite magmatism. *Contrib Mineral Petrol* 160:489–510
- Burke EAJ (2001) Raman microspectrometry of fluid inclusions. *Lithos* 55:139–158
- Caracas R, Bobocoiu E (2011) The WURM project—a freely available web-based repository of computed physical data for minerals. *Am Mineral* 96:437–443
- D'Ippolito V, Andreozzi GB, Bersani D, Lottici PP (2015) Raman fingerprint of chromate, aluminate and ferrite spinels. *J Raman Spectrosc* 46:1255–1264
- de Faria DLA, Venâncio Silva S, de Oliveira MT (1997) Raman microspectroscopy of some iron oxides and oxyhydroxides. *J Raman Spectrosc* 28:873–878
- De Pauw E, Tack P, Lindner M, Ashauer A, Garevoet J, Vekemans B, Falkenberg G, Brenker FE, Vincze L (2020) Highly sensitive nondestructive rare earth element detection by means of wavelength-dispersive X-ray fluorescence spectroscopy enabled by an energy dispersive pn-charge-coupled-device detector. *Anal Chem* 92:1106–1113
- Dörsam G, Liebscher A, Wunder B, Franz G, Gottschalk M (2009) Crystal structure refinement of synthetic $\text{Ca}_{0.43}\text{Sr}_{0.57}[\text{SiO}_3]$ -walsstromite and walsstromite–fluid Ca–Sr distribution at upper-mantle conditions. *Eur J Mineral* 21:705–714
- Elements (2020) Raman spectroscopy in earth and planetary sciences. Pasteris JD, Beyssac O (eds) *Elements* 16:77–148
- Everall NJ (2009) Confocal Raman microscopy: performance, pitfalls, and best practice. *Appl Spectrosc* 63:245a–262a
- Fedoraeva AS, Shatskiy A, Litasov KD (2019) The join CaCO_3 – CaSiO_3 at 6 GPa with implication to Ca-rich lithologies trapped by kimberlitic diamonds. *High Press Res* 39:547–560
- Frezzotti ML, Tecce F, Casagli A (2012) Raman spectroscopy for fluid inclusion analysis. *J Geochem Explor* 112:1–20
- Fries M, Steele A (2010) Raman spectroscopy and confocal Raman imaging in mineralogy and petrography. *In: Confocal Raman Microscopy*. Springer, p 111–135
- Gasparik T, Wolf K, Smith CM (1994) Experimental determination of phase relations in the CaSiO_3 system from 8 to 15 GPa. *Am Mineral* 79:1219–1222
- Gasparik T, Tripathi A, Parise JB (2000) Structure of a new Al-rich phase, $[\text{K}, \text{Na}]_{0.9}[\text{Mg}, \text{Fe}]_2[\text{Mg}, \text{Fe}, \text{Al}, \text{Si}]_6\text{O}_{12}$, synthesized at 24 GPa. *Am Mineral* 85:613–618
- Gautron L, Kesson SE, Hiberson WO (1996) Phase relations for $\text{CaAl}_2\text{Si}_2\text{O}_8$ (anorthite composition) in the system CaO – Al_2O_3 – SiO_2 at 14 GPa. *Phys Earth Planet Inter* 97:71–81
- Gillet P, Sautter V, Harris J, Reynard B, Harte B, Kunz M (2002) Raman spectroscopic study of garnet inclusions in diamonds from the mantle transition zone. *Am Mineral* 87:312–317
- Grimsditch MH, Anastassakis E, Cardona M (1978) Effect of uniaxial stress on the zone-center optical phonon of diamond. *Phys Rev B: Condens Matter* 18:901–904
- Gu T, Wang W (2018) Optical defects in milky type IaB diamonds. *Diamond Relat Mater* 89:322–329
- Gurney JJ, Helmstaedt HH, Richardson SH, Shirey SB (2010) Diamonds through time. *Econ Geol* 105:689–712
- Haggerty SE (1999) A diamond trilogy: superplumes, supercontinents, and supernovae. *Science* 285:851–860
- Harte B (2010) Diamond formation in the deep mantle: the record of mineral inclusions and their distribution in relation to mantle dehydration zones. *Mineral Mag* 74:189–215
- Harte B, Hudson NFC (2013) Mineral associations in diamonds from the lowermost upper mantle and uppermost lower mantle. *Proceedings of 10th International Kimberlite Conference Vol 1*, p 235–253
- Hayman P, Kopylova M, Kaminsky F (2005) Lower mantle diamonds from Rio Soriso (Juina area, Mato Grosso, Brazil). *Contrib Mineral Petrol* 149:430–445
- Hemley RJ (1987) Pressure dependence of Raman spectra of SiO_2 polymorphs: α -quartz, coesite, and stishovite. *In: High-Pressure Research in Mineral Physics*. Vol 39. Manghnani MH, Syono Y, (eds). AGU, Washington, D. C., p 347–359
- Hirose K, Takafuji N, Sata N, Ohishi Y (2005) Phase transition and density of subducted MORB crust in the lower mantle. *Earth Planet Sci Lett* 237:239–251
- Hope GA, Woods R, Munce CG (2001) Raman microprobe mineral identification. *Miner Eng* 14:1565–1577
- Howell D, Wood IG, Dobson DP, Jones AP, Nasdala L, Harris JW (2010) Quantifying strain birefringence halos around inclusions in diamond. *Contrib Mineral Petrol* 160:705–717
- Howell D, Wood IG, Nestola F, Nimis P, Nasdala L (2012) Inclusions under remnant pressure in diamond: a multi-technique approach. *Eur J Mineral* 24:563–573
- Irifune T, Ringwood AE (1987) Phase transformations in primitive morb and pyrolite compositions to 25 GPa and some geophysical implications. *In: High-Pressure Research in Mineral Physics*. Manghnani MH, Syono Y, (eds). Tokyo/American Geophysical Union, Terra Scientific Publishing Company, Washington DC, p 231–242

- Irfune T, Ringwood AE (1993) Phase transformations in subducted oceanic crust and buoyancy relationships at depths of 600–800 km in the mantle. *Earth Planet Sci Lett* 117:101–110
- Irfune T, Ringwood AE, Hibberson WO (1994) Subduction of continental crust and terrigenous and pelagic sediments: an experimental study. *Earth Planet Sci Lett* 126:351–368
- Izraeli ES, Harris JW, Navon O (1999) Raman barometry of diamond formation. *Earth Planet Sci Lett* 173:351–360
- Joswig W, Paulus EF, Winkler B, Milman V (2003) The crystal structure of CaSiO_3 -walsstromite, a special isomorph of wollastonite-II. *Z Kristallogr Cryst Mater* 218:811
- Kalugina AD, Zedgenizov DA (2020) Raman discrimination of garnet inclusions in Siberian diamonds. *J Raman Spectrosc* 51:1438–1444
- Kaminsky F (2012) Mineralogy of the lower mantle: A review of ‘super-deep’ mineral inclusions in diamond. *Earth Sci Rev* 110:127–147
- Kaminsky FV, Wirth R (2011) Iron carbide inclusions in lower-mantle diamond from Juina, Brazil. *Can Mineral* 49:555–572
- Kaminsky F, Wirth R, Matsyuk S, Schreiber A, Thomas R (2009) Nyerereite and nahcolite inclusions in diamond: evidence for lower-mantle carbonatitic magmas. *Mineral Mag* 73:797–816
- Kawashima Y, Katagiri G (1999) Observation of the out-of-plane mode in the Raman scattering from the graphite edge plane. *Phys Rev B Condens Matter* 59:62–64
- Kemppinen LI, Kohn SC, Parkinson JJ, Bulanova GP, Howell D, Smith CB (2018) Identification of molybdenite in diamond-hosted sulphide inclusions: Implications for Re–Os radiometric dating. *Earth Planet Sci Lett* 495:101–111
- Kim Y, Lee EJ, Roy S, Sharbiri AS, Ranz L-G, Dieing T, Kim J (2020) Measurement of lateral and axial resolution of confocal Raman microscope using dispersed carbon nanotubes and suspended graphene. *Curr Appl Phys* 20:71–77
- Koivula JJ (2000) The MicroWorld of Diamonds. Gemworld International, Inc., Northbrook, IL
- Kolesov BA, Geiger CA (1998) Raman spectra of silicate garnets. *Phys Chem Miner* 25:142–151
- Komabayashi T, Omori S (2006) Internally consistent thermodynamic data set for dense hydrous magnesium silicates up to 35 GPa, 1600 °C: Implications for water circulation in the Earth’s deep mantle. *Phys Earth Planet Inter* 156:89–107
- Konzett J, Frost DJ (2009) The high P – T stability of hydroxyl-apatite in natural and simplified MORB—an experimental study to 15 GPa with implications for transport and storage of phosphorus and halogens in subduction zones. *J Petrol* 50:2043–2062
- Konzett J, Rhede D, Frost DJ (2011) The high PT stability of apatite and Cl partitioning between apatite and hydrous potassic phases in peridotite: an experimental study to 19 GPa with implications for the transport of P, Cl and K in the upper mantle. *Contrib Mineral Petrol* 163:277–296
- Kubo A, Suzuki T, Akaogi M (1997) High pressure phase equilibria in the system CaTiO_3 – CaSiO_3 : stability of perovskite solid solutions. *Phys Chem Miner* 24:488–494
- Kudoh Y, Kanzaki M (1998) Crystal chemical characteristics of α - CaSi_2O_5 , a new high pressure calcium silicate with five-coordinated silicon synthesized at 1500°C and 10 GPa. *Phys Chem Miner* 25:429–433
- Lafore B, Schmitz S, Vekemans B, Rudloff J, Garrevoet J, Tucoulou R, Brenker FE, Martinez-Criado G, Vincze L (2014) Nanoscopic X-ray fluorescence imaging of meteoritic particles and diamond inclusions. *Anal Chem* 86:12369–12374
- Lafuente B, Downs RT, Yang H, Stone N (2015) The power of databases: The RRUFF project. *In: Highlights in Mineralogical Crystallography*. Armbruster T, Danisi RM (eds). W. De Gruyter, Berlin, p 1–30
- Litasov KD, Ohtani E (2007) Effect of water on the phase relations in Earth’s mantle and deep water cycle. *In: Geological Society of America Special Papers*. Vol 421. Ohtani E (ed), p 115–156
- Liu L-g, Memagh TP, Jaques AL (1990) A mineralogical Raman spectroscopy study on eclogitic garnet inclusions in diamonds from Argyll. *Contrib Mineral Petrol* 105:156–161
- Logvinova A, Wirth R, Fedorova E, Sobolev N (2008) Nanometre-sized mineral and fluid inclusions in cloudy Siberian diamonds: new insights on diamond formation. *Eur J Mineral* 20:317–331
- Ma C, Tschauner O, Beckett JR, Rossman GR, Prescher C, Prakapenka VB, Bechtel HA, MacDowell A (2018) Liebermannite, KAlSi_3O_8 , a new shock-metamorphic, high-pressure mineral from the Zagami Martian meteorite. *Meteorit Planet Sci* 53:50–61
- Mazzucchelli ML, Bumley P, Angel RJ, Morganti S, Domeneghetti MC, Nestola F, Alvaro M (2018) Elastic geothermobarometry: corrections for the geometry of the host–inclusion system. *Geology* 46:231–234
- McMillan P, Akaogi M, Ohtani E, Williams Q, Nieman R, Sato R (1989) Cation disorder in garnets along the $\text{Mg}_3\text{Al}_2\text{Si}_3\text{O}_{12}$ – $\text{Mg}_4\text{Si}_4\text{O}_{12}$ join: an infrared, Raman and NMR study. *Phys Chem Miner* 16:428–435
- Memagh TP, Trudu AG (1993) A laser Raman microprobe study of some geologically important sulphide minerals. *Chem Geol* 103:113–127
- Murayama JK, Nakai S, Kato M, Kumazawa M (1986) A dense polymorph of $\text{Ca}_3(\text{PO}_4)_2$: a high pressure phase of apatite decomposition and its geochemical significance. *Phys Earth Planet Inter* 44:293–303
- Murri M, Mazzucchelli ML, Campomenosi N, Korsakov AV, Prencipe M, Mihailova BD, Scambelluri M, Angel RJ, Alvaro M (2018) Raman elastic geobarometry for anisotropic mineral inclusions. *Am Mineral* 103:1869–1872
- Nasdala L, Schmidt C (2020) Applications of Raman spectroscopy in mineralogy and geochemistry. *Elements* 16:99–104
- Nasdala L, Brenker FE, Glinnemann J, Hofmeister W, Gasparik T, Harris JW, Stachel T, Reese I (2003) Spectroscopic 2D-tomography: Residual pressure and strain around mineral inclusions in diamonds. *Eur J Mineral* 15:931–935

- Nasdala L, Hofmeister W, Harris JW, Glinnemann J (2005) Growth zoning and strain patterns inside diamond crystals as revealed by Raman maps. *Am Mineral* 90:745–748
- Navon O, Wirth R, Schmidt C, Jablon BM, Schreiber A, Emmanuel S (2017) Solid molecular nitrogen (δ -N₂) inclusions in Juina diamonds: Exsolution at the base of the transition zone. *Earth Planet Sci Lett* 464:237–247
- Németh P, Leinenweber K, Ohfuji H, Groy T, Domanik KJ, Kovács JJ, Kovács JS, Buseck PR (2017) Water-bearing, high-pressure Ca-silicates. *Earth Planet Sci Lett* 469:148–155
- Nestola F (2017) Inclusions in super-deep diamonds: windows on the very deep Earth. *Rend Lincei-Mat Appl* 28:595–604
- Nestola F, Burnham AD, Peruzzo L, Tauro L, Alvaro M, Walter MJ, Gunter M, Anzolini C, Kohn SC (2016) Tetragonal Almandine-Pyrope Phase, TAPP: finally a name for it, the new mineral jeffbenite. *Mineral Mag* 80:1219–1232
- Nestola F, Korolev N, Kopylova M, Rotiroti N, Pearson DG, Pamato MG, Alvaro M, Peruzzo L, Gurney JJ, Moore AE, Davidson J (2018) CaSiO₃ perovskite in diamond indicates the recycling of oceanic crust into the lower mantle. *Nature* 555:237–241
- Neuville DR, de Ligny D, Henderson GS (2014) Advances in Raman spectroscopy applied to earth and material sciences. *Rev Mineral Geochem* 78:509–541
- Nimis P, Alvaro M, Nestola F, Angel RJ, Marquardt K, Rustioni G, Harris JW, Marone F (2016) First evidence of hydrous silicic fluid films around solid inclusions in gem-quality diamonds. *Lithos* 260:384–389
- Ohtani E, Litasov K, Suzuki A, Kondo T (2001) Stability field of new hydrous phase, δ -AlOOH, with implications for water transport into the deep mantle. *Geophys Res Lett* 28:3991–3993
- Ohtani E, Hirao N, Kondo T, Ito M, Kikegawa T (2005) Iron-water reaction at high pressure and temperature, and hydrogen transport into the core. *Phys Chem Miner* 32:77–82
- Ono S, Ohishi Y, Isshiki M, Watanuki T (2005) In situ X-ray observations of phase assemblages in peridotite and basalt compositions at lower mantle conditions: Implications for density of subducted oceanic plate. *J Geophys Res Solid Earth* 110:B02208
- Palot M, Jacobsen SD, Townsend J, Nestola F, Marquardt K, Miyajima N, Harris J, Stachel T, McCammon C, Pearson D (2016) Evidence for H₂O-bearing fluids in the lower mantle from diamond inclusion. *Lithos* 265:237–243
- Pasteris JD, Beyssac O (2020) Welcome to Raman spectroscopy: Successes, challenges, and pitfalls. *Elements* 16:87–92
- Pearson DG, Brenker FE, Nestola F, McNeill J, Nasdala L, Hutchison MT, Matveev S, Mather K, Silversmit G, Schmitz S, Vekemans B (2014) Hydrous mantle transition zone indicated by ringwoodite included within diamond. *Nature* 507:221–224
- Ringwood AE (1958) Olivine–spinel transition in fayalite. *GSA Bull* 69:129–130
- Rudloff-Grund J, Brenker F, Marquardt K, Howell D, Schreiber A, O'Reilly S, Griffin W, Kaminsky F (2016) Nitrogen nano-inclusions in milky diamonds from Juina area, Mato Grosso State, Brazil. *Lithos* 265:57–67
- Schiferl D, Nicol M, Zaug JM, Sharma SK, Cooney TF, Wang S-Y, Anthony TR, Fleischer JF (1997) The diamond ¹³C/¹²C isotope Raman pressure sensor system for high-temperature/pressure diamond-anvil cells with reactive samples. *J Appl Phys* 82:3256–3265
- Sharma SK, Mao HK, Bell PM, Xu JA (1985) Measurement of stress in diamond anvils with micro-Raman spectroscopy. *J Raman Spectrosc* 16:350–352
- Shirey SB, Cartigny P, Frost DJ, Keshav S, Nestola F, Nimis P, Pearson DG, Sobolev NV, Walter MJ (2013) Diamonds and the geology of mantle carbon. *Rev Mineral Geochem* 75:355–421
- Shirey S, Smit K, Pearson D, Walter M, Aulbach S, Brenker F, Bureau H, Burnham A, Cartigny P, Chacko T, Frost D (2019) Diamonds and the mantle geodynamics of carbon: Deep mantle carbon evolution from the diamond record. *In: Deep Carbon: Past to Present*. Orcutt BN, Daniel I, Dasgupta R, (eds). Cambridge University Press, Cambridge, p 89–128
- Smit KV, Shirey SB, Stern RA, Steele A, Wang W (2016) Diamond growth from C–H–N–O recycled fluids in the lithosphere: Evidence from CH₄ micro-inclusions and $\delta^{13}\text{C}$ – $\delta^{15}\text{N}$ –N content in Marange mixed-habit diamonds. *Lithos* 265:68–81
- Smith EM (2021) Raman spectra catalogue for inclusions in diamond. <https://doi.org/10.7939/DVN/JEHGBW>
- Smith EM, Wang W (2017) Diamond with concentric inclusions. *Gems Gemol* 53:228
- Smith EM, Kopylova MG, Frezzotti ML, Afanasiev VP (2014) N-rich fluid inclusions in octahedrally-grown diamond. *Earth Planet Sci Lett* 393:39–48
- Smith EM, Kopylova MG, Frezzotti ML, Afanasiev VP (2015) Fluid inclusions in Ebelyakh diamonds: Evidence of CO₂ liberation in eclogite and the effect of H₂O on diamond habit. *Lithos* 216–217:106–117
- Smith EM, Vendrell C, Johnson P (2016a) Coesite inclusions with filaments in diamond. *Gems Gemol* 52:410–412
- Smith EM, Shirey SB, Nestola F, Bullock ES, Wang J, Richardson SH, Wang W (2016b) Large gem diamonds from metallic liquid in Earth's deep mantle. *Science* 354:1403–1405
- Smith EM, Shirey SB, Wang W (2017) The very deep origin of the world's biggest diamonds. *Gems Gemol* 53:388–403
- Smith EM, Shirey SB, Richardson SH, Nestola F, Bullock ES, Wang J, Wang W (2018) Blue boron-bearing diamonds from Earth's lower mantle. *Nature* 560:84–87
- Sobolev NV, Fursenko BA, Goryainov SV, Shu J, Hemley RJ, Mao A, Boyd FR (2000) Fossilized high pressure from the Earth's deep interior: the coesite-in-diamond barometer. *PNAS* 97:11875–11879
- Stachel T (2014) Diamond. *In: Geology of Gem Deposits, Second Edition*. Groat LA (ed) Mineralogical Association of Canada, p 1–28

- Stachel T, Harris JW (2008) The origin of cratonic diamonds – Constraints from mineral inclusions. *Ore Geol Rev* 34:5–32
- Stachel T, Harris JW, Brey GP, Joswig W (2000) Kankan diamonds (Guinea) II: lower mantle inclusion parageneses. *Contrib Mineral Petrol* 140:16–27
- Stachel T, Brey G, Harris JW (2005) Inclusions in sublithospheric diamonds: glimpses of deep earth. *Elements* 1:73–78
- Suzuki A, Ohtani E, Kamada T (2000) A new hydrous phase δ -AlOOH synthesized at 21 GPa and 1000 °C. *Phys Chem Miner* 27:689–693
- Tappert R, Tappert MC (2011) *Diamonds in nature: a guide to rough diamonds*. Springer Science & Business Media
- Thomson AR, Kohn SC, Bulanova GP, Smith CB, Araujo D, Walter MJ (2016) Trace element composition of silicate inclusions in sub-lithospheric diamonds from the Juina-5 kimberlite: Evidence for diamond growth from slab melts. *Lithos* 265:108–124
- Tomilenko AA, Ragozin AL, Shatskii VS, Shebanin AP (2001) Variation in the fluid phase composition in the process of natural diamond crystallization. *Dokl Earth Sci* 379:571–574
- Tschauner O (2019) High-pressure minerals. *Am Mineral* 104:1701–1731
- Tschauner O, Huang S, Greenberg E, Prakapenka VB, Ma C, Rossman GR, Shen AH, Zhang D, Newville M, Lanzirotti A, Tait K (2018) Ice-VII inclusions in diamonds: Evidence for aqueous fluid in Earth's deep mantle. *Science* 359:1136–1139
- Urakawa S, Kondo T, Igawa N, Shimomura O, Ohno H (1994) Synchrotron radiation study on the high-pressure and high-temperature phase relations of $KAlSi_3O_8$. *Phys Chem Miner* 21:387–391
- von Huene R, Scholl DW (1991) Observations at convergent margins concerning sediment subduction, subduction erosion, and the growth of continental crust. *Rev Geophys* 29:279–316
- Walter MJ, Bulanova GP, Armstrong LS, Keshav S, Blundy JD, Gudfinnsson G, Lord OT, Lennie AR, Clark SM, Smith CB, Gobbo L (2008) Primary carbonatite melt from deeply subducted oceanic crust. *Nature* 454:622–625
- Walter MJ, Kohn SC, Araujo D, Bulanova GP, Smith CB, Gaillou E, Wang J, Steele A, Shirey SB (2011) Deep mantle cycling of oceanic crust: Evidence from diamonds and their mineral inclusions. *Science* 334:54–57
- Woodland AB, Girmis AV, Bulatov VK, Brey GP, Höfer HE (2020) Breyite inclusions in diamond: experimental evidence for possible dual origin. *Eur J Mineral* 32:171–185
- Workman RK, Hart SR, Jackson M, Regelous M, Farley KA, Blusztajn J, Kurz M, Staudigel H (2004) Recycled metasomatized lithosphere as the origin of the Enriched Mantle II (EM2) end-member: Evidence from the Samoan volcanic chain. *Geochem Geophys Geosyst* 5:Q04008
- Wunder B, Rubie DC, Ross CR, Medenbach O, Seifert F, Schreyer W (1993) Synthesis, stability, and properties of $Al_2SiO_4(OH)_2$: A fully hydrated analogue of topaz. *Am Mineral* 78:285–297
- Wunder B, Andrut M, Wirth R (1999) High-pressure synthesis and properties of OH-rich topaz. *Eur J Mineral* 11:803–813
- Xie X, Minitti ME, Chen M, Mao H-K, Wang D, Shu J, Fei Y (2003) Tuite, γ - $Ca_3(PO_4)_2$: a new mineral from the Suizhou L6 chondrite. *Eur J Mineral* 15:1001–1005
- Xue X, Kanzaki M, Fukui H, Ito E, Hashimoto T (2006) Cation order and hydrogen bonding of high-pressure phases in the Al_2O_3 - SiO_2 - H_2O system: An NMR and Raman study. *Am Mineral* 91:850–861
- Xue X, Kanzaki M, Fukui H (2010) Unique crystal chemistry of two polymorphs of topaz-OH: A multi-nuclear NMR and Raman study. *Am Mineral* 95:1276
- Zhai S, Yamazaki D, Xue W, Ye L, Xu C, Shan S, Ito E, Yoneda A, Yoshino T, Guo X, Shimozuku A (2013) P - V - T relations of γ - $Ca_3(PO_4)_2$ tuite determined by in situ X-ray diffraction in a large-volume high-pressure apparatus. *Am Mineral* 98:1811

